Pentacene homojunctions: Electron and hole transport properties and related photovoltaic responses

Kentaro Harada, Moritz Riede, and Karl Leo*
Institut für Angewandte Photophysik, Technische Universität Dresden, 01062 Dresden, Germany

Olaf R. Hild
Fraunhofer Institut für Photonische Mikrosysteme, Maria-Reiche-Straße 2, 01109 Dresden, Germany

C. Michael Elliott
Chemistry Department, Colorado State University, Fort Collins, Colorado 80523, USA
(Received 18 January 2008; revised manuscript received 22 April 2008; published 28 May 2008)

We report on organic *p-i-n* homojunctions composed of differently doped vacuum-deposited pentacene layers. We observe a remarkably high built-in voltage of 1.65 V. An analysis of the current-voltage characteristics under dark and illuminated conditions reveals that the open-circuit voltage is directly related to the built-in voltage and that the recombination process is influenced by the distinct charge transport properties of electrons and holes in the pentacene film. By a comparison with *p-i-p* and *n-i-n* single-carrier homojunctions, deep trap states located around 0.63 eV below the electron transport level are shown to influence the properties.

DOI: 10.1103/PhysRevB.77.195212 PACS number(s): 73.40.Lq, 73.50.Pz, 73.61.Ph, 82.45.Aa

I. INTRODUCTION

Organic semiconductors have recently gained much attention due to applications in a new class of optoelectronic devices such as large-area organic light-emitting diodes (OLEDs) or low-cost organic solar cells (OSCs). Understanding of the fundamental charge transport properties in organic thin films and the related diode characteristics in an elementary device structure is therefore of great significance for the further development of optoelectronic applications and improvement of energy conversion efficiencies.

The *p-n* homojunction is the archetype of semiconductor devices. Inorganic silicon *p-n* homojunctions as well as amorphous silicon *p-i-n* homojunctions have been long used for commercial solar cell applications. The relation of dark and illuminated diode characteristics to the solar cell parameters of the amorphous homojunctions has been already studied intensively in the 1980s.[1,2] In comparison, the fundamental properties of organic semiconductor junctions are still much less understood. Organic semiconductors are usually characterized by a high degree of disorder and concomitant localization of charge carriers. On the other hand, since organic semiconductors retain their electronic structures of closed molecular systems, the number of intrinsic defects in organic thin films is generally much lower than that in inorganic amorphous films having a large number of dangling bonds. It is interesting to clarify whether the characteristics of an organic homojunction follow the standard semiconductor theories represented by Shockley.[3]

The difficulty in the realization of the organic homojunctions lies in the energetics of the matrix, *p*-dopant, and *n*-dopant molecules: The charge transfer between the matrix and dopants should be efficient enough that both *p*-type and *n*-type conduction can be achieved in the same organic semiconductor matrix. For *p*-type doping, the dopant should have the lowest unoccupied molecular orbital (LUMO) located energetically near or below the highest occupied molecular orbital (HOMO) of the matrix. Analogously, the HOMO of the *n*-type dopant is required to be energetically near or above the LUMO of the matrix. These conditions are difficult to meet in the same material, since it requires very strong donor and acceptor molecules.

In the last few years, doping of organic semiconductors with molecular dopants has been investigated in detail[4–6] and has been applied in devices: e.g., highly efficient organic light-emitting diodes.[7] For *p*-type doping, it has been already shown that 2,3,5,6-tetrafluoro-tetracyano-quinodimethane (F_4-TCNQ) is an efficient acceptor molecule, which leads to very high hole concentrations of up to 10^{19} cm^{-3} in zinc-phthalocyanine (ZnPc).[8,9] For *n*-type doping, Bloom *et al.*[10] have demonstrated that the electrochemically doubly reduced (starting from the common 2+ oxidation state) form of bis(2,2′:6′,2″-terpyridine)ruthenium, $[Ru(terpy)_2]^0$, is a strong donor molecule. The neutral form of the complex has an oxidation potential of −1.7 V and Fermi energy of −1.5 V versus Ag/Ag^+ electrode of cyclic voltammograms, which roughly correspond to the absolute energy of −3.3 and −3.1 eV, respectively, from the vacuum level.[11]

In our previous work,[12] using F_4-TCNQ and $[Ru(terpy)_2]^0$ as the dopants, we have demonstrated that organic *p-i-n* homojunctions composed of *p*- and *n*-type ZnPc layers show well rectifying diode characteristics. The intrinsic interlayer is necessary to achieve a blocking junction since the rather narrow space-charge layers would cause tunneling.[13] It has been shown that the dark currents in the organic homojunctions are neither limited by space charge nor influenced by the contact work function, being free from injection barrier problems. The homojunction characteristics are adequately described by the Shockley equation with an exception concerning the temperature dependence of the diode parameters, for which inclusion of carrier localization effects is needed.

For this work, we have further developed the method for the strong *n* doping. Substitution of electron-donating alkyl groups for the methines in $[Ru(terpy)_2]^0$ yields the

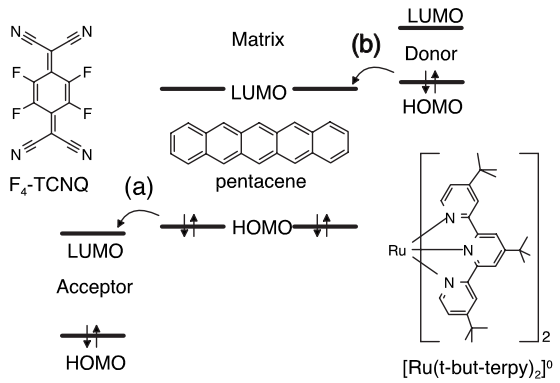

FIG. 1. Energy-level scheme of (a) *p*-type and (b) *n*-type molecular doping, together with the chemical structure of F_4-TCNQ, pentacene, and $[Ru(t\text{-but-terpy})_2]^0$.

terpyridine analog bis(4,4′,4″-tri-tert-butyl-2,2′:6′,2″-terpyridine)ruthenium, $[Ru(t\text{-but-terpy})_2]^0$. The alkyl substitution should lift the HOMO of the complex[14] 0.1–0.2 eV higher than the level of the unsubstituted ligand complex. Thus, an efficient *n* doping of matrices with relatively higher-lying LUMO becomes possible. It is thus also possible to prepare a *p-i-n* homojunction in materials with a larger energy gap.

We have chosen pentacene as the matrix for the model of our organic homojunction studies. Pentacene is one of the most thoroughly investigated organic materials with a large application potential owing to its excellent hole transport properties. While remarkably high hole mobilities have been reported for single crystals[15] and also for thin films,[16] it has been indicated that pentacene is actually an ambipolar semiconductor and the apparently low electron mobility often found in organic field-effect transistors is merely due to the low injection barrier and concomitant depletion: Indeed, comparably high field-effect mobilities of the order of 0.1 $cm^2/(V\ s)$ for both electrons and holes are achieved in thin films when the injection problem is relieved.[17,18] The long exciton diffusion length in pentacene makes it also a promising candidate for *p*-type host material in OSCs,[19–21] often combined with an *n*-type host such as C_{60}. Such an organic *p-n* heterojunction with two different host materials is much easier to fabricate since the *n* host material with relatively lower-lying LUMO does not require strong donors for *n*-type conduction. However, the open-circuit voltage of such an arrangement is limited by the LUMO of the *n* host. It is thus interesting to study the mechanism of the thermodynamic limits of the open-circuit voltage in a pentacene *p-i-n* homojunction structure. The following discussions show that the maximum open-circuit voltage achievable in the homojunction is in accordance with the built-in voltage of the junction. A large built-in voltage is due to the difference in the Fermi energies of the *p*- and *n*-type pentacene layers, induced by the efficient doping with the strong acceptor and donor molecules. Figure 1 shows the schematic image of the *p* and *n* doping of the pentracene matrix used in this study, and the chemical structure of the acceptor F_4-TCNQ and the donor $[Ru(t\text{-but-terpy})_2]^0$ are also shown.

In the following, we first discuss the energetics of the doped pentacene matrix, and then we investigate the relation between the dark and illuminated current-voltage (*J-V*) characteristics of the pentacene *p-i-n* homojunction. We also aim to elucidate the individual charge transport properties of electrons and holes in pentacene thin films using the homojunctions as the archetype of organic semiconductor devices. For these purposes, Sec. III A deals with basic characterizations of doped pentacene films by thermovoltage measurements and photoelectron spectroscopy. In Sec. III B, the dark *J-V* characteristics of the pentacene *p-i-n* homojunction are discussed. Section III C discusses the temperature and light intensity dependence of the solar cell parameters, such as open-circuit voltage V_{OC} and short-circuit current J_{SC}, of the *p-i-n* homojunction. In Sec. III D, we investigate single-carrier properties by using another type of pentacene junctions: *p-i-n* and *n-i-n* single-carrier homojunctions. The comparison of the rather different dark characteristics and photoconductivity of the two types of homojunctions leads to the conclusion that the performance of the elementary organic junctions is influenced by a presence of deep carrier trapping states.

II. EXPERIMENT

The donor compound $[Ru(t\text{-but-terpy})_2]^0$ is synthesized in an electrochemical cell at Colorado State University and kept either in vacuum or in a purified nitrogen atmosphere. The acceptor compound F_4-TCNQ is purchased (Acros Organics). The matrix material pentacene is synthesized by a unique method based on reduction of pentacene-6,13-dion as the starting compound (Institute for Organic and Macromolecular Chemistry, University of Bremen). Information on the molecular orbitals for the matrix is also provided by semiempirical PM3 calculations with HYPERCHEM. For a hole transport buffer layer, 4,4′,4″-tris(2-naththylphenylamino)-triphenylamin (TNATA) is purchased (Syntec GmbH) and used to ensure a smooth interlayer between indium tin oxide (ITO) and pentacene layers. The HOMO of TNATA lies at nearly the same level[22] as that of pentacene. The compounds F_4-TCNQ, pentacene, and TNATA are purified at least twice by vacuum gradient sublimation.

Quartz glass substrates with two vapor deposited silver contacts with a distance of 5.0 mm are used for thermovoltage measurements. A linearly graded temperature distribution (1 K/mm) across the contacts is provided by two isolated copper plates for heating and cooling of the substrates. The thermovoltage is measured *in situ* in a high-vacuum chamber (pressure $<10^{-4}$ Pa) after coevaporation of the matrix and dopants. All electrical data in this work are recorded with a source measure unit (Keithley SMU236).

The ultraviolet photoelectron spectroscopy (UPS) is performed with a hemispherical energy analyzer (SPECS PHOIBOS100). The UV light source is a helium arc lamp that provides a He (I) line at 21.22 eV. A gold foil is repeatedly cleaned by argon sputtering and then used as the common substrate for all the UPS measurements performed *in situ*.

For homojunction devices, ITO-coated glass sheets (Thin Film Device Inc., sheet resistance $<80\ \Omega/\square$) are used as the substrates. All substrates in this work are cleaned before

TABLE I. Seebeck coefficients S and energetic intervals $|E_F - E_\mu|$ obtained from thermovoltage measurements at 300 K for p-doped and n-doped pentacene samples. Doping ratios of the samples are both 2 mol %. Conductivities σ are obtained under an electric field of 40 V/cm.

Sample	S (mV/K)	$\lvert E_F - E_\mu \rvert$ (eV)	σ (S/cm)
p-Pc	0.514	0.154	6.3×10^{-4}
n-Pc	−1.016	0.305	7.5×10^{-5}

TABLE II. UPS data for doped and undoped pentacene samples. The HOMO cutoff levels are shown as the binding energy E_{bin} from the substrate work function and also in terms of E_F values with respect to the gold work function -5.27 ± 0.05 eV.

Sample	E_{bin} (±0.05 eV)	E_F (±0.1 eV)	IP (±0.1 eV)
p-Pc	0.37	−4.90	−5.08
i-Pc	0.87	−4.40	−5.03
n-Pc	2.02	−3.25	−5.10

the vacuum process by an ultrasonic treatment in acetone and ethanol and by rf-plasma treatment with oxygen radicals. Preparation of each layer is sequentially processed in ultrahigh-vacuum chambers (pressure $<10^{-5}$ Pa), and the doping ratio and layer thickness are controlled by monitoring quartz oscillator sensors. The J-V characteristics are recorded either *in situ* or in a purified nitrogen atmosphere.

Impedance measurements are performed with an *LCR* meter (HP 4284A) to confirm the relative permittivity ϵ_r of pentacene films. By comparison of several sample capacitances with different thicknesses, we have obtained $\epsilon_r=5.7$.

A sun simulator (Hoenle SOL1200) and a xenon lamp (ILC technology R150) are used as light sources for sample illumination. The light intensities are determined by an outdoor reference cell provided by the Fraunhofer Institut für Solare Energiesysteme (Freiburg, Germany). The absorption spectrum of a pentacene film is measured with a UV-vis-NIR photometer (Shimadzu UV-3100). Selective excitation of a homojunction sample is performed utilizing a set of xenon lamp and monochromator of a spectrofluorometer (SPECS FluoroMax).

III. RESULTS AND DISCUSSION

A. Energetics of the pentacene matrix

In order to study the equilibrium charge carrier statistics in doped pentacene single layers, we performed thermovoltage measurements. The Seebeck coefficient S is the average entropy per unit charge q transported along with a charge carrier. It is known that S generally depends on the Fermi energy E_F and density of states (DOS) distribution in the system.[23] For nondegenerate semiconductors, we assume that the Maxwell-Boltzmann approximation is applicable; hence, S can be described as

$$S = \frac{k_B}{q}\exp\left(\frac{E_F - E_\mu}{k_B T}\right), \tag{1}$$

where k_B is the Boltzmann constant, T is the temperature, and E_μ is the carrier transport energy. Here, the energetic interval $|E_F - E_\mu|$ implicitly includes the polaron effect[24] in a highly polarizable material. Note that for n-type semiconductors, S has a negative value. Table I summarizes the results of the thermovoltage measurements at room temperature for p-doped (p-Pc) and n-doped pentacene (n-Pc) layers together with the conductivities in the films. The Seebeck coefficient is indeed positive for p-Pc and is negative for n-Pc as is expected and confirming that even for molecularly doped layers, the mobile carrier transport is in the HOMO and LUMO, respectively, and not through the dopant states. Calculation of $|E_F - E_\mu|$ using Eq. (1) yields a value of about 0.3 eV for n-Pc, being twice the value for p-Pc. In other words, the n-type doping seems not to be as efficient as the p-type doping.

The HOMO levels and absolute E_F values in pentacene films can be confirmed by photoelectron spectroscopy. We have performed UPS measurements for n-Pc and p-Pc thin films with the same doping condition as in the thermovoltage measurements and also for an undoped pentacene thin film (i-Pc). The large sample thicknesses (20–25 nm) ensure that the UPS spectra do not originate from the interface dipole regions, but do reflect the bulk electronic structures. Knowing the gold substrate work function, we can estimate E_F of each sample from the HOMO cutoff level in the respective spectrum. The results are listed in Table II together with the ionization potentials (IPs) calculated from the HOMO cutoff and the high-binding-energy cutoff (HBEC) levels. We do not expect that only 2 mol % of doping and the corresponding change in charge density significantly alter the spectroscopic property of the bulk. Thus, the differences of the IPs between the three samples are attributed to the experimental accuracy in obtaining the HBEC levels. However, the difference in the Fermi levels between n-Pc and p-Pc, $E_{Fn}-E_{Fp}=1.65$ eV, is a definite and convincing value since these levels are well aligned to the common work function of the measurements.

The combination of the results from the thermovoltage and UPS measurements allows one to describe the complete energetics of a pentacene p-i-n homojunction as seen in Fig. 2. We assume the HOMO of the pentacene matrix to be around −5.05 eV. Although an effective carrier transport level E_μ is in general not equivalent to the DOS peak of molecular orbitals,[25] we use in this article the terms HOMO and LUMO by convention to refer to these transport levels for holes and electrons, respectively. The energy interval

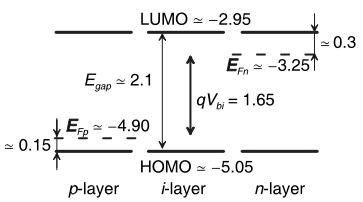

FIG. 2. Energy diagram for a pentacene p-i-n structure (energy unit in eV): E_{gap}, the energy gap; V_{bi}, the built-in voltage; E_{Fp} and E_{Fn}, the Fermi energy in the p and n layers, respectively.

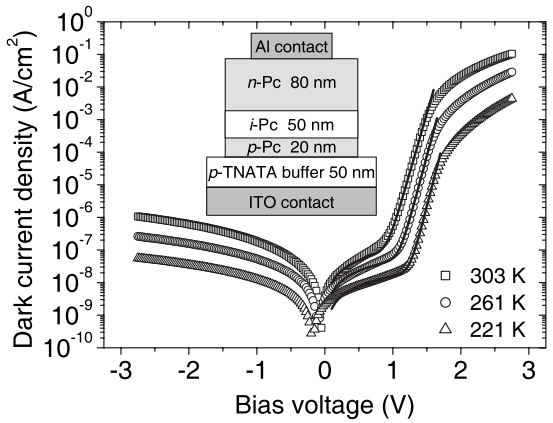

FIG. 3. Dark *J-V* characteristics of the *p-i-n* homojunction at several temperatures (open symbols). The solid lines are the calculated curves in the forward-bias region using Eq. (2). The inset shows a schematic picture of the sample structure.

$|E_F - E_\mu|$ of *p*-Pc from the Seebeck data then matches the difference between E_{Fp} and HOMO given by the UPS. This agreement justifies an estimation of the LUMO by adding $|E_F - E_\mu|$ of *n*-Pc to E_{Fn} of the UPS data. We obtain approximately −2.95 eV for the LUMO level and 2.1 eV for the energy gap E_{gap}, which are fairly consistent with values reported for pentacene films in the literature.[26,27] It is therefore reasonable to correlate the Fermi difference between the two doped layers to the built-in voltage V_{bi} in a pentacene *p-i-n* homojunction; i.e., $E_{Fn} - E_{Fp} = qV_{bi} = 1.65$ eV.

B. Dark *J-V* characteristics

A sequential vacuum deposition of *p*-Pc, *i*-Pc, and *n*-Pc leads to a *p-i-n* homojunction. Figure 3 shows the dark *J-V* characteristics of the pentacene *p-i-n* homojunction. The sample structure is also indicated as the inset of Fig. 3. The *J-V* curves exhibit a good blocking behavior in the reverse-bias region, and rectification factors of nearly 10^5 are obtained at all temperatures. In the forward-bias region below the built-in voltage, a shunt current at first appears to prevail; then, the current exponentially increases with the bias voltage. Since the effect of series resistance in this region is negligible, we only need to consider a shunt resistance R_p for the standard diode equation to describe the dark current density:

$$J_{dark} = \frac{V}{R_p} + J_0(T)\left[\exp\left(\frac{qV}{nk_BT}\right) - 1\right], \tag{2}$$

where n is the diode ideality factor. The temperature-dependent prefactor J_0 is often called the saturation current.

In the standard theory, the activation energy of J_0 is correlated with the energy gap E_{gap}. However, as already discussed in Ref. 12, J_0 of an organic homojunction cannot be associated simply with E_{gap}, and n is actually temperature dependent. It is also obvious that the shunt conductance $1/R_p$ is slightly thermally activated. Therefore, a fitting of the *J-V* curves from Eq. (2) necessarily requires a variation of these parameters as temperature is changed. A part of the fitting results are listed in Table III. We find 0.13 eV for the activation energy of $1/R_p$ and relatively large values of n increasing with decreasing temperature. Such large ideality factors around 2 infer in classical semiconductor junctions that charge carrier recombination in the *i* layer would have considerable influence. The temperature dependence of n, however, requires another explanation: The deviation from ideality can be explained by assuming that the quasiequilibrium balance between drift and diffusion currents in the disordered system is not maintained by the conventional Einstein relation[12,28–30]

TABLE III. Diode parameters at several temperatures obtained from the dark *J-V* characteristics of the *p-i-n* homojunction using Eq. (2).

T (K)	R_p (Ω cm^2)	J_0 (A/cm^2)	n
303	1.05×10^7	2.15×10^{-10}	2.30
261	2.18×10^7	1.81×10^{-12}	2.49
221	6.37×10^7	1.48×10^{-14}	2.81

$$\frac{D}{\mu} = \frac{k_BT}{q}, \tag{3}$$

where D and μ are the diffusion coefficient and drift mobility, respectively, of the charge carriers.

C. Photovoltaic properties

We now discuss the photovoltaic properties of the pentacene *p-i-n* homojunctions. As can be seen in Fig. 4, under illumination of a sun simulator, the homojunction exhibits a V_{OC} of nearly 1.1 V at room temperature, which is about 52% of the energy gap. The photocurrent is linearly dependent on the bias voltage in the range below V_{OC}, indicating that field-induced dissociation[31,32] is the dominant mechanism for the free-carrier generation. Therefore, the photocurrent density does not saturate at zero bias, yielding a relatively low J_{SC} of 32 μA/cm^2. This is a natural consequence of the homojunction structure having no specific charge separation interface in it.

Despite the low current density, the dependence of the photocurrent on light intensity and temperature gives important information on the carrier loss mechanism. Figure 5 shows J_{SC} as a function of light intensity I_L at various tem-

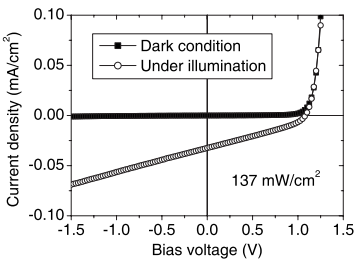

FIG. 4. *J-V* characteristics of the *p-i-n* homojunction at room temperature under illumination of 137 mW/cm^2 light from a sun simulator. The dark current is also shown for comparison.

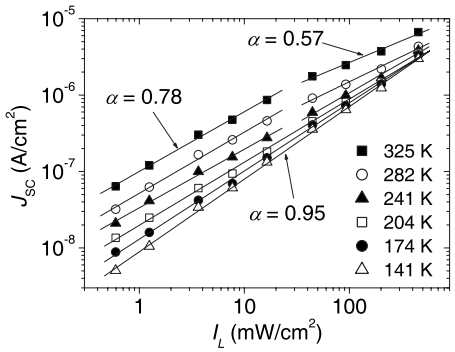

FIG. 5. Short-circuit current J_{SC} of the *p-i-n* homojunction at various temperatures as a function of illumination intensity I_L of a xenon lamp. The solid lines indicate a linear fit of the double-logarithm plots, which yield the scaling factor α at each temperature.

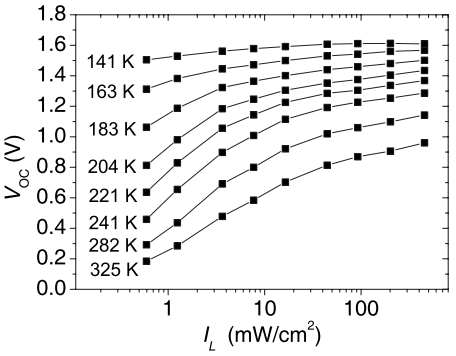

FIG. 6. Open-circuit voltage V_{OC} of the *p-i-n* homojunction at various temperatures versus illumination intensity I_L of a xenon lamp. The solid lines are guides for the eye.

peratures. It is known that in a photovoltaic system, the scaling factor α of a power law $J_{SC} \propto I_L^{\alpha}$ ranges from 0.5 to 1, depending on the carrier recombination mechanism. If oppositely charged free carriers are simultaneously present and statistically independent of each other, the carrier recombination is bimolecular[33]: In this case, α typically shows a value of 0.5. On the other hand, a linear response of J_{SC} to I_L usually means that no bimolecular, but only monomolecular recombination is taking place in a photovoltaic cell. In Fig. 5, a nonlinearity of J_{SC} to I_L is seen at high temperatures: α is about 0.78 under weak illumination, and as I_L increases, α decreases to 0.57. The reduced value of α can be attributed to the increasing number of electrons and holes both present in the *i* layer. Here, the model of space-charge-limited current (SCLC)[34] is not relevant since the *i* layer is only several tens of nanometers thick. The intermediate value of $\alpha = 0.78$ would be due to a low generation rate of free carriers, so that the bimolecular recombination cannot dominate the geminate recombination that is of monomolecular type.[26]

However, the value of α appears to approach unity as temperature is decreased and is 0.95 at 141 K. The probability of bimolecular recombination is obviously small at low temperatures, but it does not necessarily mean a decrease in the number of both types of carriers. Even at such low temperatures, J_{SC} can reach a comparably high current density of 10^{-6} A/cm^2, indicating that stronger illumination leads to much enhanced charge carrier generation at any temperature. Therefore, the behavior would be more reasonably attributed to a change in the type of recombination from a bimolecular to a monomolecular one, rather than just to a change in the free-carrier densities. A possible explanation is that one of the two types of carrier, either hole or electron, tends to become immobile when the temperature is decreased, while they are almost equally mobile at high temperatures. We will discuss in the next subsection details of the individual transport properties of electrons and holes in the homojunctions, which support this explanation.

The open-circuit voltage seen in Fig. 4 is actually lower than the expected V_{bi} of 1.65 V for the *p-i-n* homojunction. However, with a variation of temperature, a drastic change of V_{OC} is observed. Figure 6 shows V_{OC} as a function of I_L at various temperatures. It can be clearly seen that V_{OC} increases with decreasing temperature, being 1.61 V at 141 K, and appears to approach the maximum value limited by V_{bi}. The limitation is due to the fact that the electrochemical energy per electron-hole pair resulting from a strong illumination cannot be fully converted to an electrical energy under open-circuit condition.[35] On the other hand, it can be also seen that V_{OC} is generally low under weak illumination and it increases with increasing I_L. In terms of standard solar cell theory, V_{OC} is proportional to the natural logarithm of photocurrent density and, hence, to the natural logarithm of light intensity; i.e., $V_{OC} \propto \ln I_L$. However, no such relation is evidently found in the semilogarithm plots of V_{OC} versus I_L for the homojunction.

The deviation from the standard solar cell model is easily explained by comparison of the dark and illuminated *J-V* characteristics. Since V_{OC} is the point where carrier loss mechanisms equal the photogeneration rate, we can associate the dark current density J_{dark} and the photogenerated current density J_{photo} due to the fact that they are balanced at V_{OC}:

$$J_{dark}|_{V=V_{OC}} = -J_{photo}|_{V=V_{OC}}. \tag{4}$$

In the idealized case, J_{photo} is constant and equal to J_{SC}. Here, we assume that J_{photo} is not saturated, but linearly increases with electric field due to the modified Onsager model[31,32] and that the temperature dependence of the generation rate is negligible compared to the field dependence. The photocurrent density can be calculated with the values of J_{SC} and V_{OC} at each temperature. From the illuminated *J-V* characteristics (see Fig. 4), we obtain the nonsaturation factor $\beta = 0.745$ for a photocurrent density per unit voltage with respect to J_{SC}. Equation (4) can be then rewritten in an empirical form

$$\frac{V_{OC}}{R_p(T)} + J_0(T)\left[\exp\left(\frac{qV_{OC}}{n(T)k_BT}\right) - 1\right] = -J_{SC}(T)[1 - \beta V_{OC}(T)]. \tag{5}$$

Figure 7 shows the calculated J_{photo} from the right-hand side of Eq. (5) together with the measured J_{dark} in a low forward-bias range. It is evident that the characteristics of J_{photo} and J_{dark} are nearly identical at each temperature, and therefore

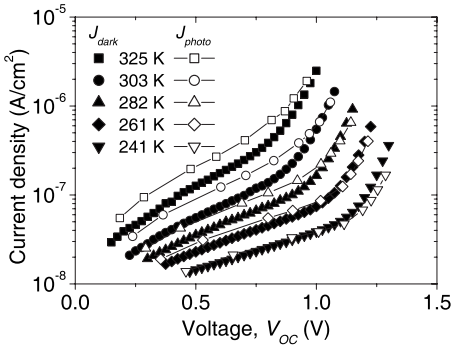

FIG. 7. Comparison of the dark current density J_{dark} (closed symbols) and the photocurrent density J_{photo} (open symbols) calculated from Eq. (5) with the J_{SC} and V_{OC} data at several temperatures.

Eq. (5) is a correct assumption. This means that in order to reach equilibrium, V_{OC} must follow a voltage regulated by J_{dark}: In other words, V_{OC} is reduced by a voltage drop due to the shunt current.

Thus, because of the relatively low photocurrent density in our *p-i-n* homojunctions, V_{OC} is inevitably lowered by the dark characteristics loss present especially at higher temperatures. However, at lower temperatures, it reveals that the thermodynamic limitation of V_{OC} is essentially determined by the built-in potential $qV_{bi}=E_{Fn}-E_{Fp}$, which we can estimate from the carrier statistics of the doped layers. The result agrees with the energy conversion model[35] for a homojunction which states that any photogenerated current driven by an excess quasi-Fermi splitting is to be compensated by currents of majority carriers in the *n* and *p* layers, generating entropy for Joule heat; i.e., the maximum V_{OC} is limited by the equilibrium condition

$$qV_{OC} \leq E_{gap} - q(S_h - S_e)T, \tag{6}$$

where S_h and S_e are the Seebeck coefficients of holes in the *p* layer and of electrons in the *n* layer, respectively. This is, however, not necessarily true for a heterojunction.

Besides the thermodynamic limitation, V_{OC} is in general limited also by the charge carrier generation rate and recombination loss mechanism, which may render the quasi-Fermi splitting lower than the built-in potential of a diode. However, whatever the final limit is, an important implication from our results is that V_{OC} of many OSCs at room temperature may be largely influenced by a balance against the dark characteristics. For example, Fig. 3 implies that the photocurrent density of our pentacene homojunction must be around 10 mA/cm^2 at room temperature in order to reach the thermodynamic limit. Such high current densities for OSCs are so far available only in heterojunction systems with excellent external quantum yields.

D. Single-carrier homojunctions

The high conductivities in *p*-Pc and *n*-Pc layers lead to Ohmic behavior of the currents even at low temperatures. Therefore, without the restriction of contact problems, we can investigate the individual carrier transport properties of holes and electrons by fabrication of *p-i-p* and *n-i-n* single-carrier organic homojunctions. For each type of device, several samples having different thicknesses of the *i* layer have been prepared. Table IV summarizes the structures and the *i* thicknesses L_i of the single-carrier homojunctions.

Figure 8 shows the comparison of *p-i-p* and *n-i-n* characteristics at room temperature. For *p-i-p* homojunctions, the currents linearly increase with increasing voltages in the low-bias range. Although a superlinear increase of the currents is seen in the high-bias range, the relation between the current densities for each sample is roughly in proportion to the electric fields in the *i* layers; i.e., $J \propto 1/L_i$. Therefore, the superlinear increase of the currents cannot be ascribed to occurrence of SCLC, but might be the consequence of an enhanced effective mobility due to the increasing charge density.[9,30,36–38] Thus, the current densities in the Ohmic regime, J_{Ohm}, are essentially expressed by

$$J_{Ohm} = \sigma_{Ohm}(V/L_i), \tag{7}$$

with a constant conductivity σ_{Ohm}.

For *n-i-n* samples, the behavior is quite different as seen in Fig. 8(b). A sample with $L_i=50$ nm shows completely Ohmic characteristics, while other samples with larger L_i show much reduced J_{Ohm} in the Ohmic regime, and the reduction of J_{Ohm} saturates for $L_i>160$ nm. Furthermore, a very steep increase of current is commonly seen in the high-voltage region for the large-L_i samples. The strong thickness dependence of the *J-V* characteristics infers a space-charge limitation of the currents. However, the relation between the *J-V* curves with different L_i does not agree with the trap-free SCLC law $J_{SCLC} \propto V^2/L_i^3$; the exponent factors for *V* and L_i are rather large, which imply the presence of electron traps. The trap-controlled SCLC is expressed, e.g., for an exponential DOS distribution, as[39]

$$J_{SCLC} \propto \frac{V^{(m+1)}}{L_i^{(2m+1)}} \quad \text{with} \quad m = \frac{T_C}{T}, \tag{8}$$

where T_C is the characteristic parameter which corresponds to the slope of the exponential tail. An attempt to fit Eq. (8)

TABLE IV. Structures and *i* thicknesses of the *p-i-p* and *n-i-n* pentacene homojunctions.

Type	Structure (thickness: nm)	L_i (nm)
p-i-p (plain)	ITO/ *p*-Pc (20)/ *i*-Pc/ *p*-Pc (85)/ Al	50, 85, 120
p-i-p (buffer)	ITO/ *p*-TNATA (50)/ *p*-Pc (20)/ *i*-Pc/ *p*-Pc (30)/ *p*-TNATA (50)/ Au	80, 160, 240
n-i-n	ITO/ *n*-Pc (20)/ *i*-Pc/ *n*-Pc (65–100)/ Al	50, 80, 110, 160, 240, 320

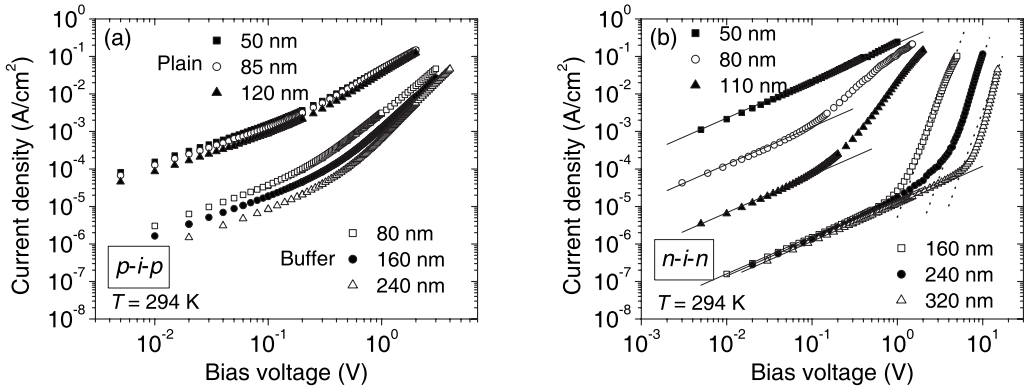

FIG. 8. Dark *J-V* characteristics of (a) *p-i-p* and (b) *n-i-n* homojunctions with a variety of *i* layer thicknesses. The solid lines in (b) are drawn by a linear fit of data to estimate σ_{Ohm}. The dotted lines in (b) for three samples are the best fit curves calculated by Eq. (8).

to J_{SCLC} data for the samples with $L_i > 160$ nm yields $m = 5.3$ at room temperature [the dotted lines in Fig. 8(b)]. However, the temperature dependence of m (not shown here) shows an inconsistency with the model described by Eq. (8). Therefore, it can be inferred that the steep increase of J_{SCLC} is not due to a gradual filling of a shallow trap distribution, but is caused by a rapid movement of the quasi-Fermi level through a filling of deep trap states.

The depth of the deep electron trap level can be estimated from the variation of σ_{Ohm}. Figure 9 shows σ_{Ohm} obtained from the slopes of the Ohmic *J-V* characteristics in Fig. 8(b), and the σ_{Ohm} data are plotted as a function of L_i. Since the Ohmic current is due to drift of free carriers, σ_{Ohm} can be written as

$$\sigma_{Ohm} = q\mu n_f \simeq q\mu N_\mu \exp\left(-\frac{E_\mu - E_\Phi}{k_B T}\right), \tag{9}$$

where n_f is the free-electron density, N_μ is the effective density of states at the transport level, and E_Φ is the quasi-Fermi level in the *i* layer. Here, we assume that n_f is different from the total injected electron density and it decreases as E_Φ moves downwards. The energy of E_Φ relative to the LUMO can be estimated from the activation energy of σ_{Ohm} (see inset of Fig. 9) by means of Eq. (9). The E_Φ level is lowered as L_i becomes larger, and it is pinned roughly at −0.63 eV for L_i exceeding 160 nm. The movement of E_Φ would correspond with the degree of electron trapping, and the pinning of E_Φ around −0.63 eV below the LUMO indicates that the deep states are energetically in the immediate vicinity.

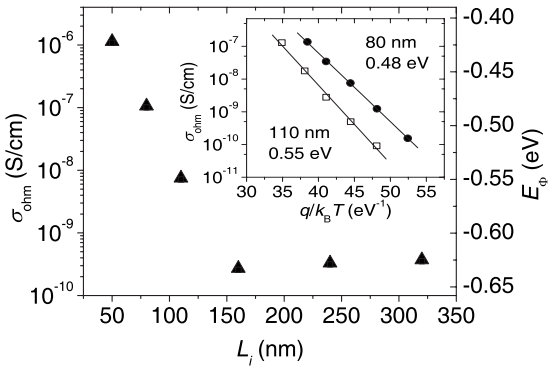

FIG. 9. Conductivity in the Ohmic regime, σ_{Ohm}, at room temperature (▲) versus L_i of the *n-i-n* homojunctions. The right-hand ordinate indicates the corresponding position of the quasi-Fermi level E_Φ measured from the LUMO. Inset shows plots for σ_{Ohm} versus reciprocal temperature of the samples with L_i=80 (●) and 110 nm (□), having an activation energy of 0.48 and 0.55 eV, respectively.

The total density of the deep trap states, N_t, is estimated as 1.5×10^{16} cm^{-3} by a consideration of the Debye length in the *i* layers. The details of the estimation are described in the Appendix.

The maximum electron mobility attainable in the *n-i-n* homojunctions can be roughly estimated as 4.3×10^{-2} cm^2/(V s) by assuming that the effective density of states, N_μ, in Eq. (9) is comparable to the molecular density 2.9×10^{21} cm^{-3}. Actually, Eq. (9) can properly describe the behavior of the σ_{Ohm} data only at lower temperatures; above room temperature, σ_{Ohm} appears to saturate at around 10^{-7} S/cm and does not exceed 10^{-6} S/cm, implying that the carrier transport in the device is limited by other factors, such as series resistance or phonon scattering. The *p-i-p* samples show also saturated conductivities of about 10^{-7} S/cm at room temperature. Therefore, we expect that electrons and holes have qualitatively the same order of effective mobilities in the *i*-Pc layer of homojunctions at sufficiently high temperatures, in agreement with literature reports.[17,18]

The existence of electron deep trap states is more evidently seen in the photoconductivity of the single-carrier devices. Figure 10 shows the change in the *J-V* characteristics of single-carrier homojunctions under illuminated conditions. The *n-i-n* sample exhibits a considerable enhancement of current density as the light intensity is increased, while the degree of the current enhancement in the *p-i-p* sample is very small. It is therefore obvious that for the *n-i-n* sample, a filling of the deep states by excitation of molecules readily enlarges the portion of free electrons that contributes to the drift currents.

In order to confirm the energetic level E_t of the deep trap states, we have performed a monochromatic excitation of the *n-i-n* sample. The current response is shown in Fig. 11 as a function of the excitation energy, together with the absorp-

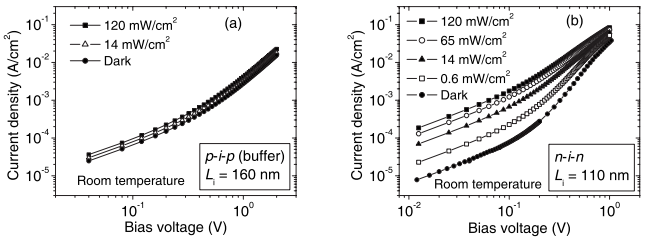

FIG. 10. Change in the *J-V* characteristics by illumination of light from a sun simulator with a variety of light intensities for the (a) *p-i-p* and (b) *n-i-n* homojunctions with L_i=160 and 110 nm, respectively.

tion spectrum of a pentacene thin film for comparison. A small photocurrent already seen at lower excitation energies infers a small probability of electronic transitions between gap states. It should be noted, however, that a steep increase of the photocurrent arises for a subtle increase of the absorption shoulder, implying that the trap filling dominantly occurs through an electron transfer from the singlet state of a molecule to a neighboring trap site. The efficient charge transfer would suggest that E_t is indeed located at a deeper level than the exciton binding energy.

The origin of the deep states is at present unknown. Such electron traps located at similar energy levels have been reported for pentacene films utilizing deep-level transient spectroscopy.[40] It is known that oxygen- and hydrogen-induced impurities such as pentacenequinone[15] and dihydropentacene[41] are typically present in pentacene compounds. However, molecular orbital calculations indicate that the LUMO levels of these impurities are located above that of pentacene host; they are basically inert for electron transport. Therefore, we speculate that, in general, no gap state active as electron trap is introduced by these chemical impurities unless the pentacene film is strongly stressed by a bias field[41,42] or irradiation.[43]

The overall energy scheme obtained in this work is summarized as the diagram in Fig. 12. By the filling of a neighboring deep state via a Frenkel exciton state, a geminate pair may be formed. The increasing number of the germinate pairs would not directly contribute to a hole current density, but it does promote a drift current at the electron transport level in pentacene.

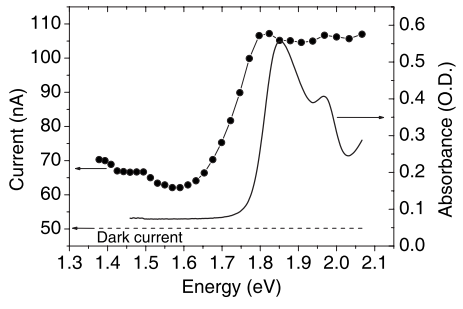

FIG. 11. Change in the currents (●) by excitation of monochromatic light for the *n-i-n* homojunction (L_i=110 nm) at a constant bias. The dashed line indicates the dark current level of the sample with the same bias. The solid line shows the absorption spectrum of a pentacene thin film 100 nm thick.

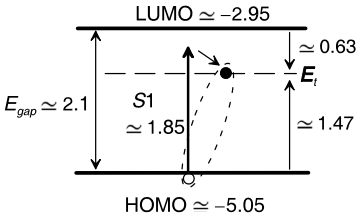

FIG. 12. Schematic energy diagram of a pentacene thin film, assuming the existence of electron trapping states whose energetic position E_t deeper than the singlet-exciton level *S*1.

IV. CONCLUSION

We investigate the properties of pentacene *p-i-n* homojunctions obtained by molecular *p*- and *n*-type doping by coevaporation of suitable dopants. A strong *n*-doping effect with the neutralized complex $[\mathrm{Ru(t\text{-}but\text{-}terpy)_2}]^0$ is demonstrated. We show that the open-circuit voltage of the pentacene *p-i-n* homojunction is connected to the high built-in voltage of 1.65 V attained by the efficient *p*- and *n*-type doping of pentacene. The monomolecular-type recombination process found in the temperature dependence of the short-circuit current originates from the immobility of electrons at low temperatures. The existence of electron deep states is inferred from studies for single-carrier-type homojunctions. By combination of electrical and optical measurements, quantitative estimations can be given, revealing that the deep states are located around −0.63 eV below the LUMO with the total trap density 1.5×10^{16} cm^{-3}. The above conclusion supports the fact that an organic homojunction can be an archetypical device to investigate the fundamental charge transport properties and related photovoltaic effects in organic thin-film devices.

ACKNOWLEDGMENTS

The authors gratefully acknowledge D. Wöhrle and colleagues at the University of Bremen for providing the pentacene material and G. Schnurpfeil for the molecular orbital calculations. Financial support by the Deutsche Forschungsgemeinschaft (Grant No. LE 747/35-1 and Leibniz grant) is acknowledged. Support from the DOE Office of Basic Energy Sciences (C.M.E.) through Grant No. DE-FG02-04ER15591 is also acknowledged. We thank M. Pfeiffer and B. Maennig at Heliatek GmbH for helpful discussions and S. Olthof for help with the UPS measurements.

APPENDIX

The total trap density N_t can be estimated by a consideration of the Debye length in the *i* layers, assuming that the situation at thermal equilibrium is not significantly altered by application of low bias voltages. The Debye length λ_D characterizes the carrier distribution tail from the *n* sides, which would have an effect on the spatial attenuation of E_Φ. Here, λ_D is defined as

$$\lambda_D = \sqrt{\frac{\epsilon_r \epsilon_0 k_B T}{q^2 N_t}}, \tag{A1}$$

where ϵ_0 is the permittivity of free space. For a sufficiently large L_i compared to $2\lambda_D$, the electron distribution form the n sides is negligible. Therefore, most of the injected carriers are trapped by the unoccupied deep states in the i layer, leading to a pinning of E_Φ. On the other hand, when L_i is smaller than approximately $2\lambda_D$, a certain portion of the deep states at the center of the i layer are already filled due to the electron diffusion. This would lead to an increased free-carrier density and hence a variation of E_Φ under a low-bias condition. The onset of the E_Φ variation is found around $L_i = 150$ nm in Fig. 9. By inserting the critical thickness $L_i/2$ into λ_D of Eq. (A1), we obtain 1.5×10^{16} cm^{-3} for N_t.

The trap density can be also confirmed in terms of the onset of SCLC under a nonequilibrium steady state: The crossover from J_{Ohm} to J_{SCLC} occurs at the voltage V_x when the trap states are filled by the Ohmic injection[39]—i.e.,

$$V_x = \frac{qN_t L_i^2}{\epsilon_r \epsilon_0}. \tag{A2}$$

From Fig. 8(b), we find V_x approximately at 1.2, 2.8, and 5.1 V for samples with $L_i = 160$, 240, and 320 nm, respectively. Calculations using Eq. (A2) commonly give a value of $N_t = 1.5 \times 10^{16}$ cm^{-3} for each sample, which is consistent with the aforementioned estimation.

*leo@iapp.de

[1] M. Hack and M. Shur, J. Appl. Phys. **58**, 997 (1985).
[2] S. S. Hegedus, N. Salzman, and E. Fagan, J. Appl. Phys. **63**, 5126 (1988).
[3] W. Shockley, Bell Syst. Tech. J. **28**, 435 (1949).
[4] J. Endo, T. Matsumoto, and J. Kido, Jpn. J. Appl. Phys., Part 2 **41**, L358 (2002).
[5] W. Gao and A. Kahn, Appl. Phys. Lett. **79**, 4040 (2001).
[6] K. Walzer, B. Maennig, M. Pfeiffer, and K. Leo, Chem. Rev. **107**, 1233 (2007).
[7] G. He, M. Pfeiffer, K. Leo, M. Hofmann, J. Birnstock, R. Pudzich, and J. Salbeck, Appl. Phys. Lett. **85**, 3911 (2004).
[8] M. Pfeiffer, A. Beyer, T. Fritz, and K. Leo, Appl. Phys. Lett. **73**, 3202 (1998).
[9] B. Maennig, M. Pfeiffer, A. Nollau, X. Zhou, K. Leo, and P. Simon, Phys. Rev. B **64**, 195208 (2001).
[10] C. J. Bloom, C. M. Elliott, P. G. Schroeder, C. B. France, and B. A. Parkinson, J. Phys. Chem. B **107**, 2933 (2003).
[11] S. Trasatti, Pure Appl. Chem. **58**, 955 (1986).
[12] K. Harada, A. G. Werner, M. Pfeiffer, C. J. Bloom, C. M. Elliott, and K. Leo, Phys. Rev. Lett. **94**, 036601 (2005).
[13] J. Blochwitz, T. Fritz, M. Pfeiffer, K. Leo, D. M. Alloway, P. A. Lee, and N. R. Armstrong, Org. Electron. **2**, 97 (2001).
[14] We use the term "HOMO of the neutralized complex" to refer to its oxidation potential $(1^+/0)$.
[15] O. D. Jurchescu, J. Baas, and T. T. M. Palstra, Appl. Phys. Lett. **84**, 3061 (2004).
[16] S. Lee, B. Koo, J. Shin, E. Lee, H. Park, and H. Kim, Appl. Phys. Lett. **88**, 162109 (2006).
[17] R. Schmechel, M. Ahles, and H. von Seggern, J. Appl. Phys. **98**, 084511 (2005).
[18] Th. B. Singh, F. Meghdadi, S. Günes, N. Marjanovic, G. Horowitz, P. Lang, S. Bauer, and N. S. Sariciftci, Adv. Mater. **17**, 2315 (2005).
[19] S. Yoo, B. Domercq, and B. Kippelen, Appl. Phys. Lett. **85**, 5427 (2004).
[20] A. K. Pandey, S. Dabos-Seignon, and J.-M. Nunzi, Appl. Phys. Lett. **89**, 113506 (2006).
[21] Z. R. Hong, R. Lessmann, B. Maennig, Q. Huang, K. Harada, M. Riede, and K. Leo (unpublished).
[22] Y. Shirota and H. Kageyama, Chem. Rev. **107**, 953 (2007).
[23] H. Fritzsche, Solid State Commun. **9**, 1813 (1971).
[24] A. von Mühlenen, N. Errien, M. Schaer, M.-N. Bussac, and L. Zuppiroli, Phys. Rev. B **75**, 115338 (2007).
[25] H. Bässler, Phys. Status Solidi B **175**, 15 (1993).
[26] M. Pope and C. E. Swenberg, *Electronic Processes in Organic Crystals and Polymers* (Oxford University Press, New York, 1999), pp. 74 and 481.
[27] J. Lee, S. S. Kim, K. Kim, J. H. Kim, and S. Im, Appl. Phys. Lett. **84**, 1701 (2004).
[28] R. Richert, L. Pautmeier, and H. Bässler, Phys. Rev. Lett. **63**, 547 (1989).
[29] S. D. Baranoversuskii, T. Faber, F. Hensel, and P. Thomas, Phys. Status Solidi B **205**, 87 (1998).
[30] Y. Roichman, Y. Preezant, and N. Tessler, Phys. Status Solidi A **201**, 1246 (2004).
[31] L. Onsager, Phys. Rev. **54**, 554 (1938).
[32] R. R. Chance and C. L. Braun, J. Chem. Phys. **59**, 2269 (1973).
[33] P. Langevin, Ann. Chim. Phys. **28**, 289 (1903).
[34] V. D. Mihailetchi, J. Wildeman, and P. W. M. Blom, Phys. Rev. Lett. **94**, 126602 (2005).
[35] P. Würfel, *Physics of Solar Cells: From Principles to New Concepts* (Wiley-VCH, Weinheim, 2005), p. 93.
[36] G. Horowitz, R. Hajlaoui, and P. Delannoy, J. Phys. III **5**, 355 (1995).
[37] M. C. J. M. Vissenberg and M. Matters, Phys. Rev. B **57**, 12964 (1998).
[38] W. F. Pasveer, J. Cottaar, C. Tanase, R. Coehoorn, P. A. Bobbert, P. W. M. Blom, D. M. de Leeuw, and M. A. J. Michels, Phys. Rev. Lett. **94**, 206601 (2005).
[39] M. A. Lampert and P. Mark, *Current Injection in Solids* (Academic Press, New York, 1970), p. 25.
[40] Y. S. Yang, S. H. Kim, J.-I. Lee, H. Y. Chu, L.-M. Do, H. Lee, J. Oh, T. Zyung, M. K. Ryu, and M. S. Jang, Appl. Phys. Lett. **80**, 1595 (2002).
[41] J. E. Northrup and M. L. Chabinyc, Phys. Rev. B **68**, 041202(R) (2003).
[42] G. Gu, M. G. Kane, J. E. Doty, and A. H. Firester, Appl. Phys. Lett. **87**, 243512 (2005).
[43] R. Plugaru, C. Anghel, and A. M. Ionescu, in *Proceedings of CAS 2006 International Semiconductor Conference*, edited by D. Dascalu and A. Rusu (IEEE, New York, 2006), Vol. 2, p. 315.